

THE H I CONTENT OF THE VIRGO CLUSTER GALAXIES

J. M. Solanes¹

Because of its proximity and richness on late-type galaxies, the Virgo cluster has been the subject of numerous studies exploring the effect of the intracluster environment on galaxy evolution. First discovered nearly three decades ago by Davies & Lewis (1973), the neutral hydrogen (HI) deficiency of the Virgo galaxies is now a well-established observational phenomenon also observed on many other rich clusters. A number of studies on the neutral hydrogen 21-cm line of Virgo cluster galaxies—from the lenticular and largest spiral types through the faintest dwarf irregulars—show that a significant number of these objects have lost a substantial fraction of their atomic hydrogen and are HI-deficient when compared with galaxies of the same optical properties in less dense environments.

1. INTRODUCTION

Nowadays, the wealth of HI data gathered for the Virgo cluster region makes it possible to obtain a reliable description of the pattern of neutral gas deficiency on supercluster scales. I will present here a recent evaluation of the large-scale radial run of the HI deficiency on the Virgo I cluster (VIC) region traced by the giant spiral population, as well as of the distribution of this property in the two- and three-dimensional space, obtained from the combination of 21-cm data with Tully-Fisher (TF) distance measurements. I will also attempt to provide suggestive evidence that objects with high HI deficiencies are not exclusively confined to the Virgo cluster proper, but can be also observed both in a background galaxy group at ~ 25 – 30 Mpc from us (possible related to the classical W' cloud) and in various galaxies lying in the frontside of the cluster at line-of-sight (LOS) radial distances less than 15 Mpc.

A dynamical model for the collapse and rebound of spherical shells under the point mass and radial flow approximations will be used to demonstrate that it is not unfeasible that some galaxies far from the cluster, including those in the gas-deficient group

well to its background, went through the cluster core a few Gyr ago. The implications would be: (1) that a substantial fraction of the HI-deficient spirals in the VIC region might have been deprived of their neutral hydrogen by interactions with the hot intracluster medium; and (2) that objects spending a long time outside the cluster cores might keep the gas deficient status without significantly altering their morphology.

2. OBSERVATIONAL DATA

2.1. Sample Selection and Homogenization

Our data set Solanes et al. (2002) is based on the complete spiral sample used by Yasuda et al. (1997) to study the structure of the Virgo cluster from *B*-band TF distances. This sample has been supplemented by data from seven other TF studies of the Virgo cluster. We have selected from the original catalogs only galaxies with heliocentric radial velocities below the well-defined gap near 3000 km s^{-1} that neatly isolates the Virgo region in redshift space (Binggeli et al. 1993). In addition, we have focused on galaxies located in the region bounded by $12\text{h} \leq \text{R.A.} \leq 13\text{h}$ and $0^\circ \leq \text{Decl.} \leq +25^\circ$ (equatorial coordinates are referred to the B1950.0 equinox), which encompasses the *Virgo Cluster Catalog* (VCC) survey boundary and is centered on the classical VIC (de Vaucouleurs 1961). The selection procedure implies that all galaxies included in our catalog are expected to have peculiar motions influenced by the central mass concentration of the cluster.

The initial selection of Virgo galaxies includes a total of 198 objects representing virtually all spiral galaxies used to date in the application of the TF relation to study the VIC region. Since TF distances from different data sets are not always consistent, the average of the measurements available for each object does not necessarily provide the best estimate of the galaxy distances. Thus, the all catalogs have been reduced to a homogeneous system by eliminating systematic differences among the different sources by means of a recursive procedure (see Solanes et al. 2002, for details). A Table, available through the Virgo web page, lists the individual and homogenized distance moduli for the 198 galaxies initially selected.

¹Departament d'Enginyeria Informàtica i Matemàtiques, Universitat Rovira i Virgili. Av. Paisos Catalans, 26; 43007 Tarragona, Spain. (jsolanes@etse.urv.es).

2.2. The 21-cm sample

Since irregular and bulge-dominated galaxies may give unreliable TF distances and/or HI content measurements, the morphologies of the galaxies have been re-examined after the homogenization of the distance moduli in order to pick up only those with Hubble types ranging from $T = 1$ (Sa) to $T = 9$ (Sm), as given in the *Third Reference Catalogue of Bright Galaxies* (RC3).

The principal source for the HI line fluxes is the *Arecibo General Catalog* (AGC), maintained by Riccardo Giovanelli and Martha P. Haynes at Cornell University, which contains an extensive compilation of 21-cm-line measurements collected from a large number of sources. HI flux measures for a few of objects were also taken from *A General Catalog of HI Observations of Galaxies* (Huchtmeier & Richter 1989) and from the *Lyon-Meudon Extragalactic Database* (LEDA). All the observational values have been corrected for the effects of random pointing errors, source extent, and internal HI absorption following Haynes & Giovanelli (1984), except the (nine) non-AGC fluxes and the only non-detection, V0522, which have been corrected only for internal HI self-absorption. The AGC is also adopted as the source of other observational parameters required by our study, such as the equatorial coordinates of the galaxies, their visual optical diameters, which are involved in the determination of the HI deficiency, and their heliocentric radial velocities, which are transformed to systemic velocities, v_{sys} , by referring them to the kinematic frame of the Local Group, taken equal to 308 km s^{-1} towards $(l, b) = (105^\circ, -7^\circ)$ (Yahil et al. 1977).

On the other hand, for the HI-line width we have adopted the inclination-corrected values of the line width at 20% level of the line-profile peak, W_{20}^c , listed in Yasuda et al. (1997). For most of the galaxies that concern us here, these authors provide a set of observations standardized into line widths measured at the Arecibo circular feed following a similar process to that carried out in Solanes et al. (2002) with the distance moduli. For galaxies not included in the Yasuda et al.’s sample, we use the values of W_{20} and inclination quoted in LEDA, except for the galaxy V1043, not listed in either of these two catalogs, for which we adopt the corresponding measurements by Mould et al. (1980). Furthermore, we have excluded spiral galaxies with $W_{20}^c \leq 100 \text{ km s}^{-1}$ to reduce the error induced from turbulent disk motion. We do not find it necessary, however, to impose an inclination cut.

After all these selections, we end up with a sam-

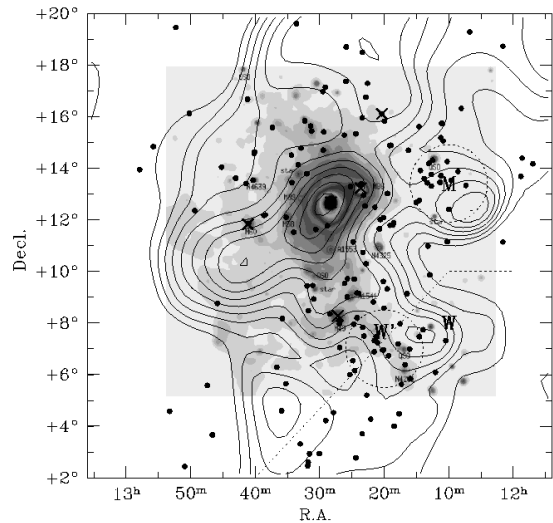


Fig. 1. Distribution in celestial coordinates of the 161 members of the 21-cm sample. The contour map of the *distance-independent* HI deficiency parameter is reproduced from Solanes et al. (2001). A grey-scaled version of the X-ray image of the central cluster region in the ROSAT all-sky-survey in the hard (0.4–2.4 keV) energy band is overlaid also on the figure. The background W, W', and M subgroups from Binggeli et al. (1993) are delineated by dotted lines. The sky positions of five dominant galaxies are marked by crosses (top to bottom: M100, M86, M87, M60, and M49). The projected location of M87 coincides with the peak of the HI deficiency and of the X-ray emission.

ple of 161 spiral galaxies with reliable HI content and distance data, hereafter called the “21-cm sample”, useful to assess the spatial distribution of the neutral gas deficiency in the VIC region. The scatter of the best fitting TF template for the 161 galaxies is 0.41 mag. Hence, the uncertainty in the distance modulus of the individual galaxies in this data set is comparable to the scatter of the most accurate TF template relations currently available.

A second table with the most relevant galaxy parameters is also available through the Virgo web page. The sky distribution of the members of the 21-cm sample is presented in Figure 1.

3. THE DIAGNOSIS OF HI DEFICIENCY

HI deficiency is often quantified by the parameter $\langle DEF \rangle$ defined as

$$\langle DEF \rangle = \langle \log M_{\text{HI}}(D_{\text{opt}}, T) \rangle - \log M_{\text{HI}}, \quad (1)$$

(Haynes & Giovanelli 1984; Solanes et al. 1996), where M_{HI} is the HI mass of the galaxy in solar

units, and the angular brackets on the right of the equal sign indicate the expected value of this quantity inferred from a sample of field galaxies of the same *optical* linear diameter D_{opt} and morphological type T .

The neutral hydrogen mass, in turn, is calculated from the expression

$$M_{\text{HI}} = 2.36 \times 10^5 d^2 F_{\text{HI}}, \quad (2)$$

where d is the observed LOS distance of the object in Mpc and F_{HI} represents the corrected HI flux density integrated over the profile width in units of Jy km s^{-1} . The most recent determinations of the expectation values for the HI mass as a function of the size and morphology of the galaxies are given in Solanes et al. (1996) in the form of linear regressions that imply power law relationships of the type $M_{\text{HI}} \propto D_{\text{opt}}^n$, with the values of n oscillating between about 1.7 for Sc's and 1.2 for earlier spiral types.

It is also possible to use a calibrator for the neutral gas deficiency not tied to the distance to the galaxies. Given that the $M_{\text{HI}} - D_{\text{opt}}$ relationships do not deviate substantially from a constant HI surface density, especially for the latest spiral types, it is reasonable to adopt the distance-independent approximation to equation (1) based on the difference of the logarithms of the expected and observed values of this latter quantity

$$\text{DEF} = \langle \log \bar{\Sigma}_{\text{HI}}(T) \rangle - \log \bar{\Sigma}_{\text{HI}}, \quad (3)$$

where $\bar{\Sigma}_{\text{HI}}$ is the mean *hybrid* HI surface density, which can be calculated directly from the ratio of the observables F_{HI} and the apparent optical diameter of the galaxy, a_{opt}^2 , given in arcmin (Solanes et al. 1996). The adopted values for $\langle \log \bar{\Sigma}_{\text{HI}}(T) \rangle$ are: 0.24 units for Sa, Sab; 0.38 for Sb; 0.40 for Sbc; 0.34 for Sc; and 0.42 for later spiral types.

4. THE DISTRIBUTION OF HI DEFICIENCY

Numerous studies (Giovanelli & Haynes 1985; Haynes & Giovanelli 1986; Magri et al. 1988; Cayatte et al. 1994; Bravo-Alfaro et al. 2000) reveal that gas-poor galaxies tend to be more abundant in the centers of rich galaxy clusters than in their periphery. Virgo is less rich and younger than the classical Abell clusters and is characterized by a lower X-ray luminosity and larger spiral fraction than Coma-like clusters. Probably as a result, although it does contain a substantial fraction of HI-deficient galaxies (Haynes & Giovanelli 1986; Yasuda et al. 1997; Solanes et al. 2001), the degree of HI deficiency is not observed to increase towards the center as

dramatically as in other rich clusters. However, because of its proximity, even strongly gas-poor galaxies remain detected, allowing precise determination of higher degrees of the HI-deficiency, whereas in more distant clusters only lower limits to this parameter can be derived.

The contour map of HI deficiency shown in Figure 1 illustrates that the maximum of the gas deficiency distribution coincides with the position of the central cD galaxy, M87, where the projected galaxy and intracluster gas densities are also the highest. But this map also reveals other zones of significant deficiency at sky positions dominated by background subclumps which lie at about twice the distance of the cluster core (Tully & Shaya 1984; Binggeli et al. 1987; Gavazzi et al. 1999) and are believed to be falling into it for the first time.

4.1. Radial Pattern

The first lines of evidence that there are a considerable number of galaxies with strong HI depletions on the outskirts of the Virgo cluster are presented by means of Figures 2 and 3. Figure 2 shows the values of DEF for the 161 members of the 21-cm sample as a function of LOS distance. This diagram illustrates that most of the galaxies with substantial deficiencies in the VIC region are localized in a broad range of projected distances, which stretches from about 10 to 30 Mpc along the LOS. A few more gas deficient objects lie beyond 40 Mpc.

By transforming the sky positions of the galaxies and their LOS distances to rectangular coordinates, we can also inspect the behavior of the HI deficiency as a function of the *three-dimensional* radial distance, r , from the center of Virgo. We adopt the standard identification of the cluster center at the position of M87, given by the sky coordinates ($12^{\text{h}}28^{\text{m}}3, 12^{\circ}40'$) and a distance modulus of 31.11 mag quoted in LEDA which translates to a LOS distance of 16.7 Mpc. The results are shown in Figure 3, where we use two different representations to calculate the radial run of the HI deficiency: one based on the parameter F_{DEF} , which measures the relative populations of deficient and normal spirals, and the other based directly on the averaged values of HI deficiency. In both cases the data have been binned into annuli containing 16 galaxies per ring, with the final bin having 17, in order to increase the statistical weight of the scarcer low- and high-distance objects.

For small values of the 3D clustercentric distance, $r \lesssim 4$ Mpc, the radial behavior of the gas deficiency is consistent with the pattern exhibited by the composite sample of 11 HI-deficient clusters in-

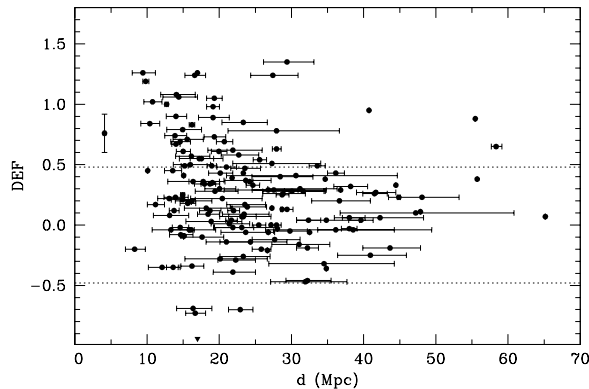


Fig. 2. Individual values of DEF for the 161 members of the 21-cm sample as a function of the LOS distance. Dotted lines show 2 times the standard deviation shown by the values of this parameter in field galaxies. Horizontal error bars represent the 1σ uncertainties of the distances quoted in the literature with respect to the calculated mean values. The filled triangle marks the distance to M87 quoted in LEDA. The vertical error bar in the point closest to us shows an estimate of the typical uncertainty of the individual values of DEF expected from random errors in the determination of the observables a_{opt}^2 , F_{DEF}^c , and T , that enter in the calculation of this parameter.

investigated in Solanes et al. (2001): it decreases almost monotonically with increasing distance from M87, implying that peak of the HI deficiency distribution coincides with the cluster center. But at greater distances this tendency is broken by a series of secondary maxima—more conspicuous in the radial run of F_{DEF} due to its higher sensitivity to localized enhancements—, showing that localized regions of gas deficiency in the VIC region can also be found well beyond the typical clustercentric distance of $\sim 3h^{-1}$ Mpc where where this property approaches normalcy in other HI-deficient clusters and where the hot X-ray emitting intracluster medium is concentrated. Be aware, however, of the fact that this same sort of careful analysis of HI deficiency at large clustercentric distances has not been performed on other clusters. So, it is not unfeasible that the differences in the radial pattern can be explained simply by the bias that arises from Virgo’s proximity which leads to (a) much larger number of 21-cm observations, (b) more stringent values of DEF, and (c) more accurate TF distance estimates.

The central peak in the radial pattern of the HI deficiency is essentially the result of the accumulation of highly deficient galaxies in the interval of

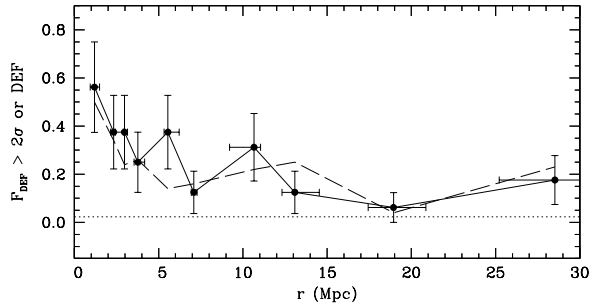


Fig. 3. Run of the fraction of spirals with $\text{DEF} > 2\sigma$ with three-dimensional radial distance from the center of the Virgo cluster. Vertical error bars correspond to 1σ confidence Poisson intervals. The abscissas show medians and interquartile ranges of the bins in distance determined from 16 galaxies, with the remainder one added to the last bin. The horizontal dotted line is the expectation value of F_{DEF} for field spirals if DEF follows a gaussian distribution. The long-dashed curve illustrates the radial run of the medians of the binned number distributions in the measured DEF.

LOS distances ranging from 16–17 Mpc up to 21–22 Mpc. This range coincides with the distribution of the bright ellipticals associated with the cluster core (Neilsen & Tsvetanov 2000). The second local maxima visible in the radial run of F_{DEF} is produced by galaxies with LOS distances $\lesssim 15$ Mpc, while the peak most distant from the cluster core obeys to the grouping of several objects with extreme deficiencies at LOS distances between about 25 and 30 Mpc from us.

Previous studies by Fukugita et al. (1993); Yasuda et al. (1997); Federspiel et al. (1998), among others, have shown that the Virgo spiral distribution is strongly elongated along the LOS. The impressions obtained above from the distribution of HI deficiency, although crude, provide further evidence for the large depth in LOS distance of the Virgo spirals, which we now see that is also reflected in the gaseous deficiency. Hence, in contrast to what it is commonly assumed, *not all the HI-poor objects in the VIC region reside in the neighborhood of the cluster core.*

4.2. Three-dimensional Distribution

Traditionally the determination of the structure of the Virgo cluster region has relied on the morphological characteristics of its associated galaxies

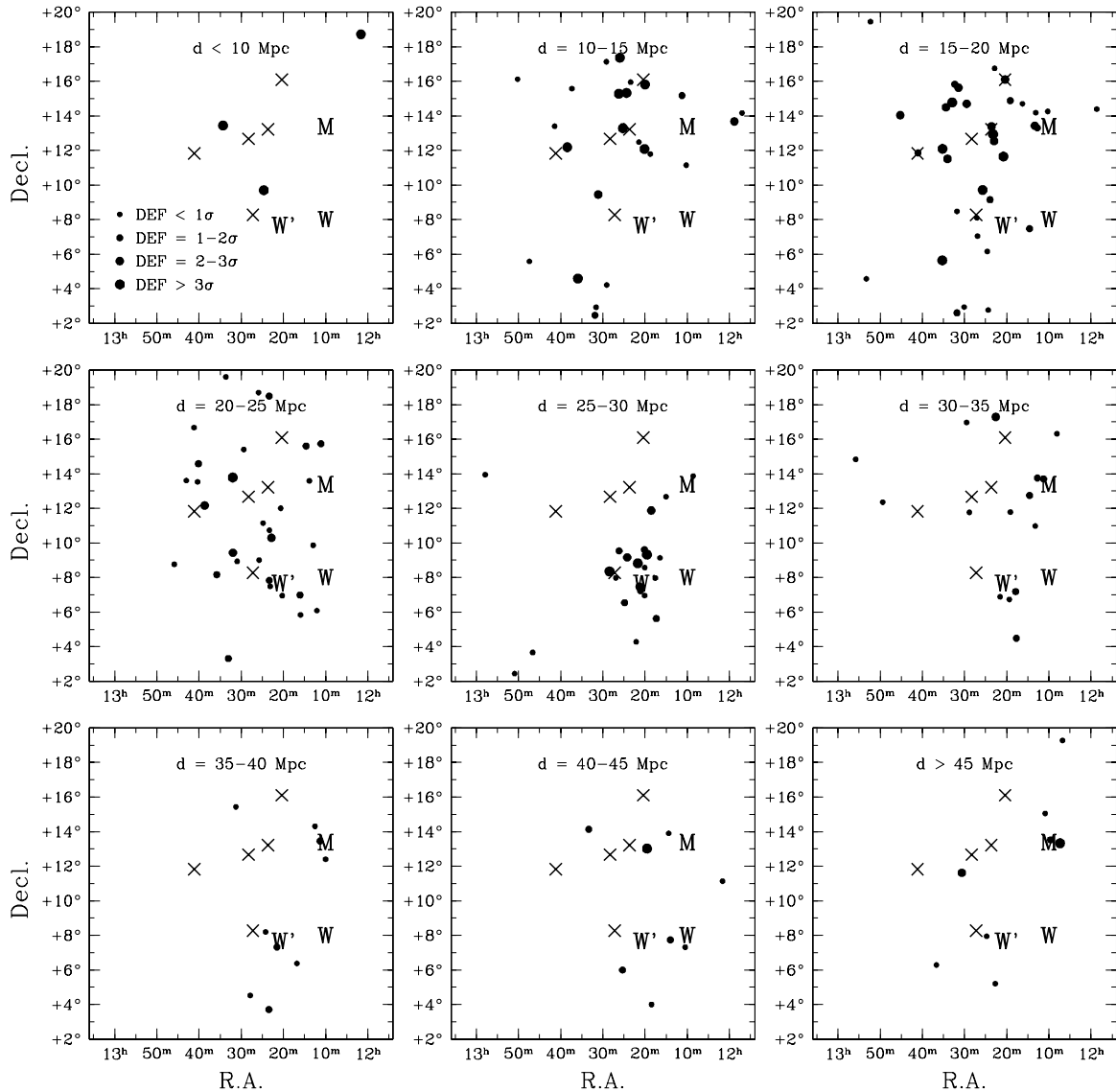


Fig. 4. Sky distribution of the Virgo spirals for specific ranges of the LOS distance. The size of the symbols correlates with the HI deficiency of the galaxies measured in units of the mean standard deviation for field objects ($= 0.24$). Crosses and uppercase letters have the same meaning as in Fig. 1.

serving as distance indicators, supplemented by velocity information (de Vaucouleurs 1961; Binggeli et al. 1985; Binggeli et al. 1993). In VCC, for instance, the galaxy morphology and membership are strongly coupled, to the point that, when the membership status is changed (because of the measured radial velocity) the Hubble type is often redefined. Given the well-defined kinematical gap behind the Virgo galaxy concentration at $\sim 3000 \text{ km s}^{-1}$, this technique isolates the cluster region from the (far)

background, but can only provide a fuzzy view of its complex morphology, especially in regions where several candidate substructures overlap in projected space and velocity (notably around the western cluster side, defining what it is known as the “spoiled” area).

Some progress toward a more precise determination of the internal structure of the Virgo cluster region and improved membership assignments is now beginning to emerge from the incorporation of

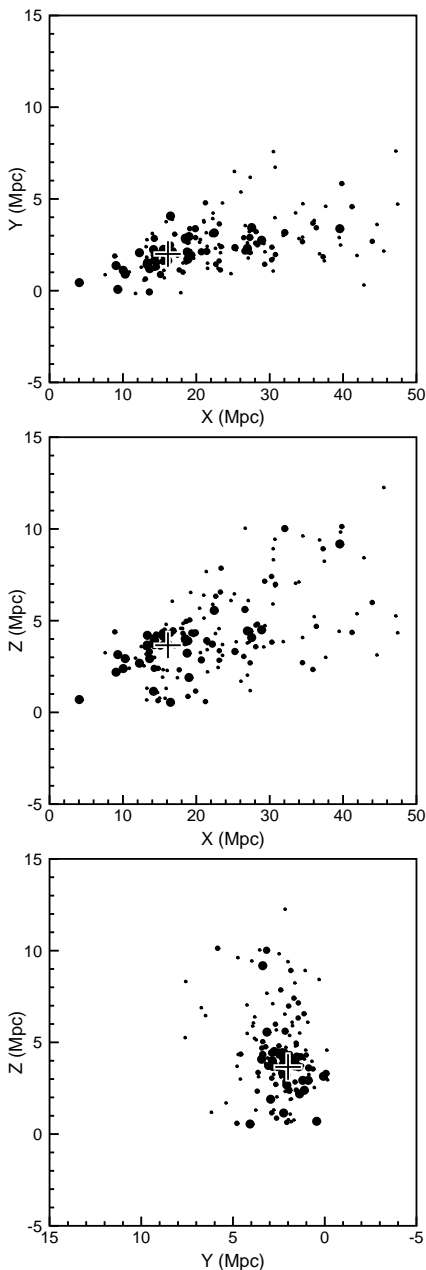


Fig. 5. Distribution of the VIC spirals in the three main planes of the rectangular equatorial coordinate system. As in Figure 4, the symbol size indicates the relative degree of HI deficiency. The large cross in each panel marks the position of M87.

spatial information based on distance measurement methods capable of determining individual galaxy distances to a precision comparable to the inter-group separations. Recent studies relying on TF,

SBF, or fundamental plane distance measurement techniques (Yasuda et al. 1997; Gavazzi et al. 1999; Neilsen & Tsvetanov 2000) have produced quite an elaborate set of substructures and opened a debate on the original group membership assignments of numerous galaxies—a detailed historical account of the studies on the structure of the Virgo cluster can be found, for instance, in Fouqué et al. (2001). In essence, however, they have confirmed the robustness of the original subdivision inferred from imaging and recessional velocity data that splits the VIC region essentially in two major central subclusters and three peripheral groups (cf. Fig. 1). The largest galaxy concentration dominates the northern part of the Virgo region and coincides with the brightest giant elliptical, M87, which also appears to be the center of the X-ray emission (Böhringer et al. 1994). This main subunit, which will be referred to here as the M87 subcluster, is supposed to trace the cluster core, which might not be virialized. In fact, Binggeli et al. (1993); Böhringer et al. (1994); Schindler et al. (1999), found evidence of dynamical disturbances that could be explained by the ongoing merging of two galaxy systems: one associated with M87 itself and the other with the pair of elliptical galaxies M86/M84. Another giant elliptical, M49, marks the center of the other major Virgo galaxy concentration, hereafter the M49 subcluster, located southwards from the M87 subcluster. The M49 subcluster appears to be connected towards the southwest with the W' and W background clouds (de Vaucouleurs 1961), forming a continuous chain that extends up to roughly twice the distance of the M87 subcluster (interestingly enough, a tenuous bridge of X-ray luminous gas can be seen in Fig. 1 connecting the M49 subcluster with the W'/W cloud region). Finally, in the northwest and at about the distance of the W cloud, there is another well-defined background cloud named M (Ftclas et al. 1984).

4.2.1. Spherical Coordinates

The tomographic presentation of the galaxy distribution shown in Figure 4 clearly demonstrates that the center of gravity of the HI deficiency distribution moves from north to south as the distance increases, consistently following the structure of the Virgo cluster described above. The major concentration of HI-deficient spirals is seen in the distance range of 15–20 Mpc encircling the position of M87. Numerous gas-deficient objects are detected also in the panels corresponding to the distance ranges of 10–15 Mpc and 25–30 Mpc. In the latter, these galaxies are essentially concentrated between the

southern edge of the M49 subcluster and the W'/W cloud region, while in the former they tend to be located to the north of M87. Some of the gas poor galaxies in the near distance slice could be former companions of M86 ejected at high speeds to relatively high clustercentric distances because of the falling of this subclump into the cluster (Solanés et al. 2001; Vollmer et al. 2001). The intermediate range of $20 < d < 25$ Mpc is composed mainly of galaxies with moderate neutral gas deficiencies spreaded more or less uniformly over all the sky. Although the uncertainties in the distance estimates do not permit a neat separation of the different Virgo substructures, it is interesting to note that the majority of the objects in the HI-deficient galaxy clustering seen at 25–30 Mpc also have systemic velocities not dissimilar from those of the M87 subcluster, in rough agreement with the original definition of the W' cloud given in VCC (note that the W cloud is underrepresented in TF data sets). On the other hand, the marginal indications of a galaxy enhancement in the NW of the 30–35-Mpc-distance slice might correspond to the M cloud, given that the candidate galaxies exhibit systemic velocities around 2000 km s^{-1} . Beyond 35 Mpc, galaxies become progressively scarce, although with an apparent tendency to reside in the peripheral W and M cloud regions. This picture is consistent with the claims that the W and M background clouds of Virgo are twice as far away as its central subunits, with the W' cloud being somewhat closer (Binggeli et al. 1987; Yasuda et al. 1997).

A final glance at Figure 4 also shows that the gas-deficient enhancement noted in the 2D image around the region of the M cloud (cf. Fig. 1) is indeed the result of the chance superposition along the LOS of several spirals with substantial gas deficiency, but located at very different LOS distances and without any physical connection.

4.2.2. Rectangular Coordinates

A complementary characterization of the spatial structure of the VIC region can be inferred from the projected distributions of the spiral galaxies into the three main planes of the cartesian three-dimensional space visualized in Figure 5. In this plot, the xy-plane is taken parallel to the equatorial plane ($\text{Decl.} = 0^\circ$), with the x- and y-axis pointing to R.A. = 12h and 18h, respectively, and the z-axis pointing to the north—as a result, the yz-plane is nearly perpendicular to the LOS to M87, i.e., it is roughly a tangent plane to the celestial sphere. The figure allows one to appreciate the true

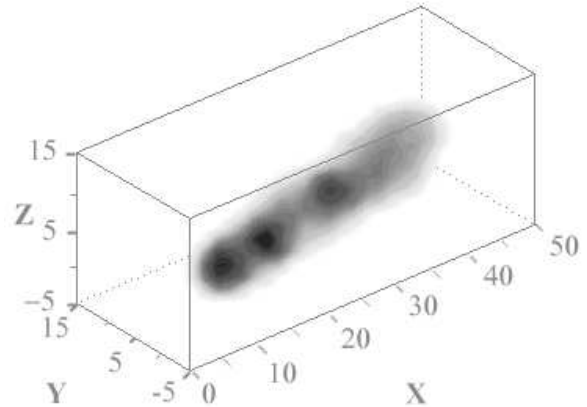


Fig. 6. Voxel projection of the 3D distribution of HI deficiency in the VIC cluster region. The plot is in rectangular equatorial coordinates. Distances are in Mpc. The xy-plane corresponds to $\text{Decl.} = 0^\circ$, the x- and y-axis point to R.A. = 12h and 18h, respectively, and the z-axis points to the north. The central enhancement is associated with the cluster (M87 is right at its center). We are at the origin of the coordinate system.

aspect of the spiral distribution in the VIC region. The most remarkable feature is the double filamentary structure that can be distinguished in the xz-plane, which is roughly perpendicular to the plane of the Local Supercluster. Notice that the galaxies with the strongest HI depletions, i.e., those with $\text{DEF} > 2\sigma$, or equivalently, a factor three reduction in the HI mass, delineate the upper filament that goes through M87 and embraces the deficient objects having the most extremal radial distances—they are indeed much more densely concentrated along the filament axis than the rest. This upper branch of the spiral distribution is pretty well aligned with the chain of bright elliptical galaxies that defines the principal axis of Virgo (Arp 1968; West & Blakeslee 2000). Emerging from this branch at around 25–30 Mpc in LOS distance there is a second filament essentially devoid of highly deficient objects.

A continuous representation in rectangular equatorial coordinates of the spatial distribution of HI deficiency in the VIC region is shown in Figure 6. This image is like a radiography in which the shade intensity informs on the average HI deficiency of the galaxy distribution observed under a given viewing angle. Three dark spots indicating the accumula-

tions of galaxies with a dearth of neutral hydrogen described above are easily identified aligned along the LOS. While the frontside enhancement of the HI deficiency is produced by gas-poor galaxies that appear relatively clustered in 3D space simply because they are nearby objects, the gas-deficient enhancement in the background arises from a compact aggregation of galaxies in the four-dimensional position-radial velocity phase space which is clearly differentiated from its surroundings. Up to 15 of the galaxies listed in the 21-cm sample are probable members of this background group. They all share similar positions in the plane of the sky ($12\text{h}15\text{m} \leq \text{R.A.} \leq 12\text{h}30\text{m}$ and $+6^\circ \leq \text{Decl.} \leq +10^\circ$) where uncertainties are negligible. In addition, 12 objects have LOS distances between 27 and 30 Mpc, and 8 of those (11 out of the initial 15) have systemic velocities between $\sim 600\text{--}1300 \text{ km s}^{-1}$. Certainly, the lack of resolution in the radial direction prevent us for claiming that we have identified a true group on a sufficiently safe basis. Yet, the fact that one third of the candidate galaxies have gas deficiencies that deviate more than 2σ from normalcy and that two of them have HI masses less than 10% of the expectation values for their morphology —characteristics that are both typical of rich cluster interiors— reinforces the impression that the compactness of these objects in the phase space is not fortuitous.

5. THE RADIAL VELOCITY FIELD

The systemic velocity-distance diagram for the VIC region plotted in Figure 7 insinuates the basic expected features: an initial steeply rising velocity-distance relation at the cluster front, a central very broad region with the maximum observed velocity amplitudes, and a final ascending part of the relation, expected to approach asymptotically the local Hubble law. Ultimately, all the available good-quality observations should be considered to define the constraints of any dynamical model of the virgo-centric velocity field. However, given the difficulties inherent to the modeling of the motions in the innermost cluster region where multiple rebounds are expected to occur, the acceptable range of models has been restricted by putting all the weight of the fits in the the two asymptotic branches of the envelope to the streaming motions with respect to the Virgo velocity. The theoretical prediction has been derived from the simple point mass model developed in Sanchis et al. (2002) for the spherical collapse of a zero-pressure fluid, which extends the calculations beyond the time until a singularity first develops until galaxies recollapse again. This is done by tak-

ing the, admittedly crude, point of view of treating galaxies as test particles moving under the influence of a central constant potential well, so the effects of shell crossing on their first orbit following rebound can be ignored. Two of the parameters of the model are allowed to vary freely: the *effective* total mass of the VIC region, M_{VIC} , and the barycentric distance from our position, whereas the velocity of the VIC in the Local Group (LG) reference frame has been fixed to 980 km s^{-1} (Teerikorpi et al. 1992).

The three solid curves in Figure 7 demonstrate the locus of the optimum model for lines-of-sight corresponding to angular separations of 4, 6, and 8 degrees. It is compelling that, in spite of the fact that the minimization relies only on a fraction of the body of the data, the best solution is able to explain a great deal of the galaxy motions around the VIC region. The good accordance between the observations and the prediction of the double-infall model is reinforced by the remarkable symmetry of the motions with respect to the local Hubble flow defined by the imaginary straight line going through the position of the LG and that of the predicted VIC barycenter. On the other hand, the best estimate $M_{\text{VIC}} = 2.8 \times 10^{15} M_\odot$ approaches closely the values $\lesssim 2 \times 10^{15} M_\odot$ inferred from modelings of the velocity field of the Local Supercluster (Tully & Shaya 1984; Fouqué et al. 2001). The acceptable barycentric distances are also well within the very poorly constrained range (16 – 24 Mpc) of VIC distances reported in the literature, although the most likely value $R_{\text{VIC}} = 21.0 \text{ Mpc}$ advocates a large-distance scale which, for a cosmological VIC velocity of 1200 km s^{-1} , brings the *local* value of the Hubble constant to about 60 km/s/Mpc . Furthermore, the best solution leads to a cosmic age $t_0 = 13.5 \text{ Gyr}$, in excellent agreement with the expansion ages of $13 \pm 1 \text{ Gyr}$ derived for the $\Omega_m = 0.3, \Omega_\Lambda = 0.7$ CDM model in the H_0 -Key Project by Freedman et al. (2001) and the more precise $t_0 = 13.6 \pm 0.2 \text{ Gyr}$ recently inferred by Sievers et al. (2002) from CMB observations.

Interestingly enough, the HI-deficient background group observed at $R \sim 28 \text{ Mpc}$ and $V \sim 1000 \text{ km s}^{-1}$ can be accommodated the same on an orbit following rebound as on a first infall trajectory. One would be therefore compelled to conclude that it is not unfeasible that these galaxies are not recent arrivals but have already plunged into the VIC center in the past. The near turnaround position of this entity in the Hubble diagram and the assumed standard harmonic oscillation movement of the galaxies around the cluster center, together with a cosmic age presumably close to 13.5 Gyr , indicate that it

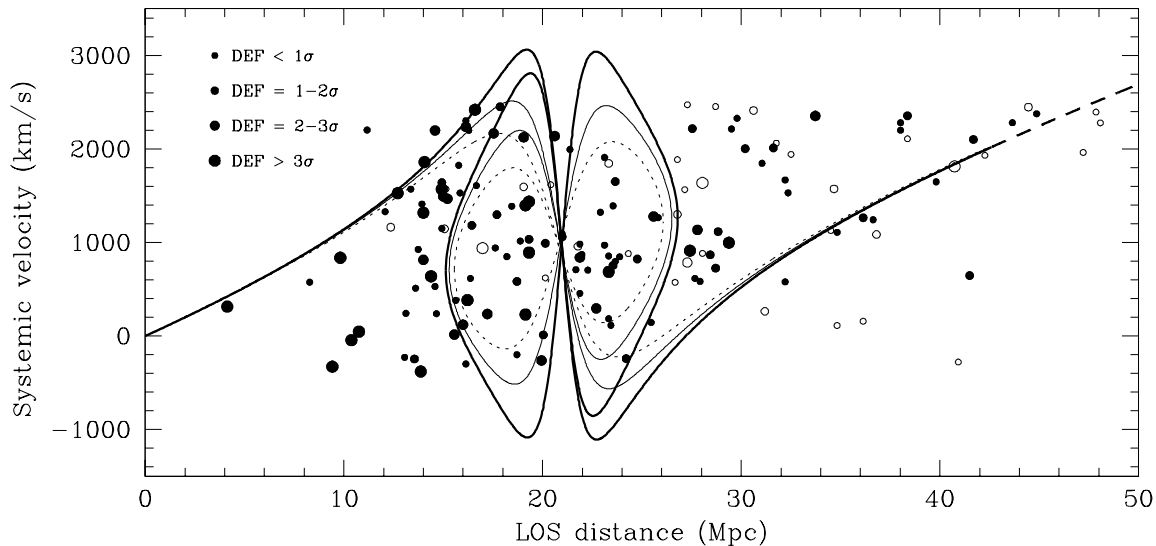


Fig. 7. Systemic velocity vs. LOS distance for spirals listed in the 21-cm sample. Solid circles identify objects with reliable distance estimates. The curves demonstrate the predicted velocities for $\theta = 4^\circ$ (thick solid), $\theta = 6^\circ$ (thin solid), and $\theta = 8^\circ$ (dotted). The dashed portion is for unbound shells. Galaxies with uncertain distances (open symbols) have been excluded from the fit.

might have experienced its first high-velocity passage² through the Virgo core about 4.5 Gyr ago.

6. CONCLUDING REMARKS

- Further progress in the knowledge of the detailed structure of the Virgo cluster needs a careful revision of TF distances—at least until Cepheid distance measurements in Virgo galaxies become more commonplace. Even after the elimination of systematic differences among published Virgo catalogs, a few galaxies still exhibit strongly inconsistent distance measurements: 16 of the 161 members of the 21-cm sample have 1σ uncertainties larger than 5 Mpc. The fact that the quoted error is small does not guarantee that the measurement is reliable. If two results clearly disagree, any average, weighted or not, is meaningless, and there is little point in performing it.
- There is now compelling evidence of the decisive participation of ram-pressure stripping, which requires high IGM densities and relative velocities, in the reduced gas abundances of the spi-

²Galaxies on first infall achieve much higher pericentric velocities than after relaxation because their turnaround radius is significantly larger. Hence they can be subject to a much higher ram pressure.

rals observed in the centers of various rich clusters, either from observational articles (Gavazzi & Jaffe 1987; Dickey & Gavazzi 1991; Solanes et al. 2001)—including the discovery of galaxies with shrunken HI disks (Cayatte et al. 1994; Bravo-Alfaro et al. 2000)—or from theoretical studies (Solanes & Salvador-Solé 1992; Fujita & Nagashima 1999; Stevens et al. 1999; Quilis et al. 2000; Vollmer et al. 2001). The finding that a number of spirals with substantial HI deficiencies lie at large radial distances from the Virgo cluster center—some are very likely members of a background subclump well behind the cluster core—may seem from the outset hard to reconcile with the proposition that this environmental process is also the cause of their gas deficiencies. However, the modeling of the velocity field around the VIC region demonstrates that characteristics such as a large virgocentric distance or a near turnaround position are not by themselves conclusive indications of a recent arrival. The substantial HI deficiency of the background subclump found in Solanes et al. (2002) may well have originated on an earlier passage of this entity through the Virgo core. A more precise knowledge of the velocity field around the VIC appears to be required to confirm or discount this possibility.

- Even if the tentative suggestion that the HI-deficient group on the backside of the VIC might not be a recent arrival is finally proven well-founded, it is still necessary finding a sensible explanation for the apparently long time ($\sim 4\text{--}5$ Gyr) its gas-poor members have maintained a substantial dearth of gas during without noticeable consequences on their morphologies: 9 of its 15 probable members are late-type spirals, whereas the 5 galaxies with the largest gaseous deficiencies have types Sb or later. Certainly, the details and chronology of the evolution of galactic properties triggered by the sweeping of the atomic hydrogen, as well as its repercussions on the star formation rate, are poorly understood.

The inconspicuous positions of the HI-deficient galaxies observed at large virgocentric distances — the gas-deficient group in the background, for instance, lies halfway between the much larger galaxy concentrations of the Virgo cluster and the background W cloud— have not encouraged systematic 21-cm surveys outside the central VIC region. I hope that this contribution provides enough grounds for changing the situation and putting the gas content of the galaxies on the outskirts of the Virgo cluster under close examination.

REFERENCES

- Arp, H. 1968, *PASP*, 80, 129
- Binggeli, B., Popescu, C., & Tammann, G.A. 1993, *Astronomy & Astrophysics Suppl. Ser.*, 98, 275
- Binggeli, B., Sandage, A., & Tammann, G.A. 1985, *AJ*, 90, 1681 (VCC)
- Binggeli, B., Tammann, G.A., & Sandage, A. 1987, *AJ*, 94, 251
- Böhringer, H., Briel, U.G., Schwarz, R.A., Voges, W., Hartner, G., & Trümper, J. 1994, *Nature*, 368, 828
- Bravo-Alfaro, H., Cayatte, V., van Gorkom, J.H., & Balkowski, C. 2000, *AJ*, 119, 580
- Cayatte, V., Kotanyi, C., Balkowski, C., & van Gorkom, J.H. 1994, *AJ*, 107, 1003
- Davies, R.D., & Lewis, B.M. 1973, *MNRAS*, 165, 231
- de Vaucouleurs, G. 1961, *ApJS*, 6, 213
- de Vaucouleurs, G., de Vaucouleurs, A., Corwin, H.G., Buta, R.J., Paturel, G., & Fouqué, P. 1991, *Third Reference Catalogue of Bright Galaxies* (New York: Springer) (RC3)
- Dickey, J.M., & Gavazzi, G. 1991, *ApJ*, 373, 347
- Ekhholm T., Lanoix, P., Teerikorpi, P., Fouqué, P., & Paturel, G. 2000, *A&A*, 355, 835 (Ekh00)
- Federspiel, M., Tammann, G.A., & Sandage, A. 1998, *ApJ*, 495, 115 (FTS98)
- Fouqué, P., Bottinelli, L., Gouguenheim, L., & Paturel, G. 1990, *ApJ*, 349, 1 (Fou90)
- Fouqué, P., Solanes, J.M., Sanchis, T., & Balkowski, C. 2001, *A&A*, 375, 770
- Freedman, W.L., et al. 2001, *ApJ*, 553, 47
- Ftclas, C., Struble, M.F., & Fanelli, M.N. 1984, *ApJ*, 282, 19
- Fujita, Y., & Nagashima, M. 1999, *ApJ*, 516, 619
- Fukugita, M., Okamura, S., & Yasuda, N. 1993, *ApJ*, 412, L13
- Gavazzi, G., Boselli, A., Scodreggio, M., Pierini, D., & Belsole, E. 1999, *MNRAS*, 304, 595 (Gav99)
- Gavazzi, G., & Jaffe, W. 1987, *A&A*, 186, L1
- Giovanelli, R., & Haynes, M.P. 1985, *ApJ*, 292, 404
- Haynes, M.P., & Giovanelli, R. 1984, *AJ*, 89, 758
- Haynes, M.P., & Giovanelli, R. 1986, *ApJ*, 306, 466
- Huchtmeier, W.K., & Richter, O.G., 1989, *A General Catalog of HI Observations of Galaxies* (Berlin: Springer)
- Kraan-Korteweg, R.C., Cameron, L.M., & Tammann, G.A. 1988, *ApJ*, 331, 620 (KCT88)
- Magri, C., Haynes, M.P., Forman, W., Jones, C., & Giovanelli, R. 1988, *ApJ*, 333, 136
- Mould, J., Aaronson, M., & Huchra, J. 1980, *ApJ*, 238, 458 (MAH80)
- Neilsen, E.H., & Tsvetanov, Z.I. 2000, *ApJ*, 536, 255
- Pierce, M.J., & Tully, R.B. 1988, *ApJ*, 330, 579 (PT88)
- Quilis, V., Moore, B., & Bower, R. 2000, *Science*, 288, 1617
- Sanchis, T., Solanes, J.M., Salvador-Solé, E., Fouqué, P. 2002, *ApJ*, submitted
- Schindler, S., Binggeli, B., & Böhringer, H. 1999, *A&A*, 343, 420
- Sievers, J.L., et al. 2002, *astro-ph/0205387*
- Solanes, J.M., Giovanelli, R., & Haynes, M.P. 1996, *ApJ*, 461, 609
- Solanes, J.M., Manrique, A., González-Casado, G., García-Gómez, C., Giovanelli, R., & Haynes, M.P. 2001, *ApJ*, 548, 97
- Solanes, J.M., & Salvador-Solé, E. 1992, *ApJ*, 395, 91
- Solanes, J.M., Sanchis, T., Salvador-Solé, E., Giovanelli, R., & Haynes, M.P. 2002, *AJ*, submitted
- Stevens, I.R., Acreman, D.M., & Ponman, T.J. 1999, *MNRAS*, 310, 663
- Teerikorpi, P., Bottinelli, L., Gouguenheim, L., & Paturel, G. 1992, *Astronomy & Astrophysics Suppl. Ser.*, 260, 17
- Tully, R.B., & Shaya, E.J. 1984, *ApJ*, 281, 31
- Vollmer, B., Cayatte, V., Balkowski, C., & Duschl, W.J. 2001, *ApJ*, 561, 708
- West, M.J., & Blakeslee, J.P. 2000, *ApJ*, 543, L27
- Yahil, A., Tammann, G.A., & Sandage, A. 1977, *ApJ*, 207, 903
- Yasuda, N., Fukugita, M., & Okamura, S. 1997, *ApJS*, 108, 417 (YFO97)